Analyst

ROYAL SOCIETY OF CHEMISTRY

PAPER

View Article Online
View Journal | View Issue

Cite this: *Analyst*, 2021, **146**, 4841

An electrochemical biosensor for the detection of pathogenic bacteria based on dual signal amplification of $Cu_3(PO_4)_2$-mediated click chemistry and DNAzymes

Hongguo Wei,[a,b] Shengjun Bu,[b] Wenguang Zhang,[b] Li Ma,[b] Xiu Liu,[b] Ze Wang,[b] Zhongyi Li,[b] Zhuo Hao,[b] Xiuxia He*[a] and Jiayu Wan *[b]

A novel electrochemical biosensor for detecting pathogenic bacteria was designed based on specific magnetic separation and highly sensitive click chemistry. Instead of enzyme–antibody conjugates, organic–inorganic hybrid nanoflowers [concanavalin A (Con A)–$Cu_3(PO_4)_2$] were used as the signal probe of the sandwich structure. The inorganic component, the copper ions of hybrid nanoflowers, was first used to amplify signal transduction for enzyme-free detection. Sodium ascorbate could dissolve $Cu_3(PO_4)_2$ of the signal probe to produce Cu^{2+}, which was subsequently converted to Cu^{+}, triggering the Cu^{+}-catalyzed alkyne–azide cycloaddition (CuAAC) reaction between azide-functionalized ssDNA (a fragment of the DNAzyme-containing sequence) and alkyne-functionalized ssDNA immobilized onto the electrode surface. As a result, the DNAzyme was immobilized onto the gold electrode, which produced a positive and stable electrical signal. An exceptional linear relationship was observed between the electrical signal and the concentration of *Salmonella typhimurium* (10^1–10^7 CFU mL^{-1}) with a detection limit of 10 CFU mL^{-1}. The developed electrochemical biosensor based on dual signal amplification of $Cu_3(PO_4)_2$-mediated click chemistry and DNAzymes exhibited good results in detecting *S. typhimurium* in milk samples.

Received 3rd June 2021,
Accepted 10th June 2021

DOI: 10.1039/d1an00982f

rsc.li/analyst

1. Introduction

Click chemistry, with advantages such as mild reaction conditions, positive selectivity, and high efficiency, has been widely researched since 2001.[1] One of the most common click reactions is the Cu^{+}-catalyzed alkyne–azide cycloaddition (CuAAC) reaction, which has been widely explored for its biological uses, such as sensing.[2,3] The main advantage of CuAAC is its dependence on the catalytic activity of Cu^{+} that is not consumed during the enzymatic reaction.[4] CuAAC has been used for signal formation in sensors for detecting Cu in water samples or for assaying reducing agents such as ascorbic acid in total proteins,[5] even at low concentrations.[6] Besides, CuAAC-based immunoassays have been developed for detecting diverse targets.[7,8] For instance, CuO nanoparticle (NP) based immunoassays have been used to detect various targets, such as alpha-fetoprotein and human immunodeficiency virus antibodies,[9] in serum samples and have presented satisfactory results.[10] Acid addition releases Cu^{2+} from the CuO NP-labeled antibody immunoassay sandwich structure, and the released Cu^{2+} is further reduced to Cu^{+} (ref. 11) that triggers a CuAAC reaction. The concentration of the target is correlated with the amount of CuO NPs in the immunoassay, and the quantity of Cu^{+} released by CuO NPs determines the value of the detection signal.[12] However, for application as a signal probe to detect targets, CuO must be conjugated to an antibody and other target-specific recognition elements, which is a complex process.[13]

Hybrid nanoflowers, consisting of inorganic (*e.g.*, phosphates such as copper phosphate ($Cu_3(PO_4)_2$)) and organic (*e.g.*, proteins) constituents, are novel hybrid NPs[14–18] that combine the functionalities of organic and inorganic materials. These NPs have attracted wide attention owing to their high efficiency, good protein stability, concise synthesis process, and higher surface-to-volume ratio that significantly enhance their catalytic activity.[19–21] Besides, the inorganic constituent forms a protective structure around the organic material, thus providing high stability to hybrid nanoflowers. Owing to their excellent performance, a variety of hybrid nanoflowers have been synthesized and applied to biosensors for assaying targets.[22,23] In a previous study, Li *et al.* synthesized glucose oxidase–horseradish peroxidase–$Cu_3(PO_4)_2$ hybrid nanoflowers as an electrochemical biosensor probe to quanti-

[a]*School of Life Science and Technology, Changchun University of Science and Technology, Changchun 130022, China. E-mail: chinese_hxx@yahoo.com.cn*
[b]*Institute of Military Veterinary Medicine, Academy of Military Medical Sciences, Changchun 130122, China. E-mail: wanjiayu@hotmail.com*

tatively detect live pathogenic bacteria.[24] Furthermore, Wu *et al.* used as-prepared DNA-$Cu_3(PO_4)_2$ hybrid nanoflowers as captors to bind signal probe DNA–invertase conjugates and a personal glucose meter for signal readout for detecting microRNA.[25] In addition, hemoglobin–$Cu_3(PO_4)_2$ hybrid nanoflowers were used as a biocatalyst to construct colorimetric/fluorescent dual biosensors for detecting H_2O_2.[26] All of the detection methods are based on the organic component of the nanoflower for the detection of target signal transformation or transmission, while the inorganic component, copper phosphate, only acts as a fixed element of the nanoflower. Tang *et al.* prepared BSA-antibody–$Cu_3(PO_4)_2$ hybrid nanoflowers as a signal enhancer for the electrochemical immunoassay of C-reactive protein, in which the inorganic component (phosphate ions) of BSA-antibody–$Cu_3(PO_4)_2$ was first used for the transduction of electrochemical readout.[24] To the best of our knowledge, copper ions (inorganic component) of hybrid nanoflowers have not been used for the transduction of signal readout for detecting the target. Our group found that the addition of sodium ascorbate can release Cu^{2+} from $Cu_3(PO_4)_2$ in hybrid nanoflowers and further reduce Cu^{2+} to Cu^{+}, which can promote a reaction that ligates a DNA probe modified by host–guest,[27] thus indicating that $Cu_3(PO_4)_2$ in hybrid nanoflowers can also act as a signal-converting substance. The readout system of the connected probe can be mainly classified into three categories: electrochemical-, visual-, and fluorescence-based.[28] Electrochemical sensors have attracted extensive attention owing to their easy operation and excellent analytical performance, and have been applied to assay target ssDNA/dsDNA with improved sensitivity.[29]

In the present study, an electrochemical immunosensor based on dual signal amplification of $Cu_3(PO_4)_2$-mediated click chemistry and DNAzymes was developed and applied to quantify pathogenic bacteria with high sensitivity, specificity, and accuracy (Scheme 1). First, a sandwich assay was used to capture the target using aptamer-modified magnetic beads (MBs) and Con A–$Cu_3(PO_4)_2$ hybrid nanoflowers. Recognition between pathogenic bacteria and MBs was accomplished by the biorecognition molecules, aptamers, with a specific three-dimensional structure, which could specifically bind to the surface of pathogenic bacteria. Owing to their higher tolerance and chemical stability than antibodies, aptamers are widely used to modify magnetic particles to capture and enrich pathogenic bacteria from complex solutions. The Con A–$Cu_3(PO_4)_2$ hybrid nanoflowers, as signal tags, played crucial roles in the portable detection of pathogenic bacteria. Recognition between pathogenic bacteria and hybrid nanoflowers was achieved by the biorecognition molecules Con A specifically binding to the surface O-antigen of pathogenic bacteria. Subsequently, MBs, the target pathogenic bacteria, and hybrid nanoflowers formed a sandwich structure. The Con A–$Cu_3(PO_4)_2$ hybrid nanoflowers, integrating the essential functions of both biological recognition and signal amplification, met the requirements of signal labels for the immunoassay of pathogenic bacteria. Next, $Cu_3(PO_4)_2$ in the hybrid nanoflowers was dissolved with EDTA to release Cu^{2+} that was further reduced to Cu^{+}. Cu^{+} triggered a CuAAC reaction between azide-functionalized ssDNA DNAzymes and alkyne-functionalized ssDNA on the electrode surface. The DNAzymes immobilized onto the gold electrode produced an electrical signal.[30]

2. Experimental

2.1. Chemicals and instruments

Streptavidin-coated MBs (average diameter, 2.8 μm) were purchased from Invitrogen (Waltham, USA), and Con A was obtained from Sangon Biotechnology, Co. (Shanghai, China).

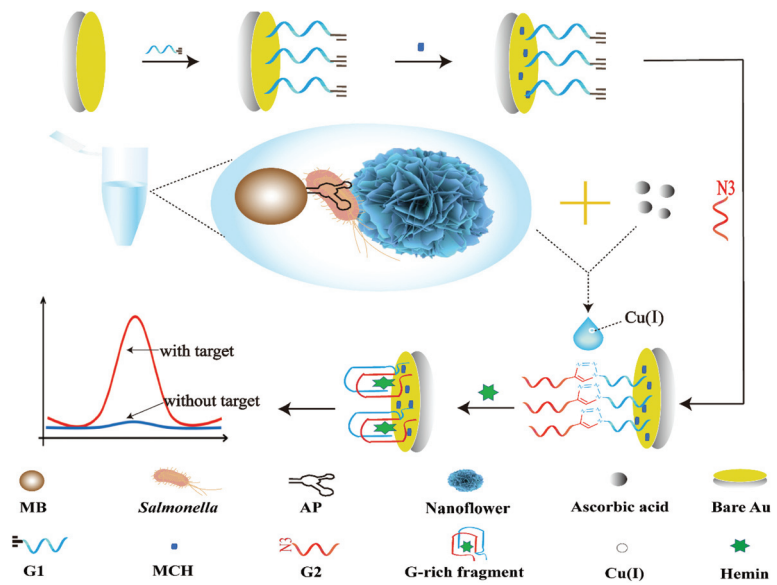

Scheme 1 Schematic illustration of the electrochemical sensor for quantitative analysis of *S. typhimurium*.

Table 1 Oligonucleotide sequences used in this study

Name	Sequence (5′–3′)
Biotin-modified aptamer	CTGATGTGTGGGTAGGTGTCGT-TGATTTCTTCTGGTGGGG
G-quadruplex-forming sequence	GTGGGTAGGGCGGGTTGGG
G1	CH≡CH–GCGGGTTGGG
G2	GTGGGTAGG–N=N=N

Iron porphyrin derivative (hemin), dimethyl sulfoxide (DMSO), copper sulfate pentahydrate ($CuSO_4{\cdot}5H_2O$), and 6-mercapto-1-hexanol (MCH) were purchased from Sigma-Aldrich (St Louis, MO, USA). The oligonucleotide sequences used in this study are listed in Table 1. The biotin-modified aptamer of *Salmonella typhimurium* was obtained from Sangon Biotech, Co. (Shanghai, China). The G-quadruplex-forming sequence was divided into two short G-rich fragments. The 3′-end of the short segment was modified with the azidyl group and the 5′-end of the other segment was modified with the acetylene group. Strains of *Staphylococcus aureus* (CICC 21600), *S. typhimurium* (CICC 24119), *Listeria monocytogenes* (CICC 21529), and *Escherichia coli* O157:H7 (CICC 21530) were obtained from the China Center for Type Culture Collection (Wuhan, China).

The CHI 660E electrochemical workstation was purchased from Shanghai Chenhua Instrument (Shanghai, China). Platinum wire was used as the auxiliary electrode, a gold electrode was used as the working electrode, and a silver electrode was used as the reference electrode. Scanning electron microscopy (SEM) images were obtained using a Zeiss Supra 40 field emission scanning electron microscope (Oberkochen, Germany). A pH meter (Horiba Co., Ltd, Kyoto, Japan) was used to adjust the pH of PBS. All aqueous solutions were prepared using ultrapure water (18.3 MΩ cm, Milli-Q; Millipore, Billerica, MA, USA).

2.2. Synthesis of Con A–$Cu_3(PO_4)_2$ hybrid nanoflowers

A one pot process was used for the synthesis of $Cu_3(PO_4)_2$ nanoflowers. To date, Cu ions have been primarily used to produce organic–inorganic hybrid nanoflowers. A total of 20 μL of $CuSO_4$ solution (180 mM) was added to 800 μL of PBS (10 mM, pH 7.4) containing 0.06 mg of Con A and shaken for 30 s. Then, the solution was incubated at 25 °C for 15 h and centrifuged at 10 000 rpm for 5 min. The precipitate obtained was dispersed in PBS (0.1 mM, pH 7.4) and centrifuged again to remove uncombined components. Finally, the collected nanoflowers were resuspended in 100 μL of PBS (0.1 mM, pH 7.4). The structure of the Con A–$Cu_3(PO_4)_2$ nanoflowers was observed under SEM.

2.3. Electrode treatment and functionalization of the sensing surface

First, the gold electrodes were immersed in freshly prepared piranha aqueous solution (peroxide solution: concentrated sulfuric acid at 1 : 3 v/v) for 20 min and polished smooth using suede with 0.05 μm aluminum slurry. Then, the electrodes were washed thoroughly with ultrapure water, immersed in ethanol for 30 min, and subjected to ultrasound treatment in deionized water for 5 min. Subsequently, the electrodes were cleaned in 0.5 M H_2SO_4 with a cyclic voltammetry (CV) range from −0.2 to 1.6 V and a scan rate of 50 mV s^{-1} until a prominent voltammetric peak was observed. Electrochemical impedance spectroscopy (EIS) was performed with parameters that included a frequency sweep range from 0.05–10^5 Hz and with a 5 mV amplitude. Differential pulse voltammetry (DPV) measurements were performed with a voltage within the range of −0.2–0.2 V, a pulse period of 0.5 s, and a modulation amplitude of 50 mV in PBS (10 mM, pH 7.0) containing 8 mM H_2O_2 and 100 mM KCl. The oligonucleotide sequence G1 (0.5 μM) was incubated with 1 mM tris (2-carboxyethyl) phosphine for 20 min at room temperature, and a droplet of 10 μL of G1 (0.5 μM) was placed onto the prepared electrode and incubated at room temperature overnight in the dark.

2.4. Detection of *S. typhimurium* using the developed electrochemical biosensor

Our developed biosensor provided a valuable and pragmatic platform for highly sensitive and selective detection of pathogenic bacteria. For the detection of *S. typhimurium*, the streptavidin-modified MB_S were mixed with 10 μL of biotin-modified aptamer (1 μM) and incubated at 37 °C for 60 min. The aptamer could specifically capture the target bacterial cells and remove the unbound residues. Subsequently, 4 μL of the hybrid nanoflowers were added to the reaction system and incubated at 37 °C for 1 h to allow the nanoflowers to combine with the target bacterial cells. After magnetic separation and washing thrice with phosphate buffer (0.1 mM, pH 7.4) to remove unbound residues, specific sandwich conjugates were acquired. Then, 0.5 μM sodium ascorbate was added to the reaction system to obtain Cu^+ that could catalyze the formation of the G-quadruplex structure. The addition of the G2 oligonucleotide sequence and Cu^+ accelerated the cycloaddition reaction between the azide and alkyne groups. A control experiment was conducted under the same conditions with PBS (0.1 mM, pH 7.4) instead of the target bacterium.

2.5. Analysis of milk samples

To verify the reliability of our developed electrochemical sensor, *S. typhimurium* suspensions at concentrations of 10^3, 10^4, and 10^5 CFU mL^{-1} were added to aseptic milk.[31,32] For the negative blank control, phosphate solution was used. The samples were examined based on the above-mentioned procedure and a calibration plot was derived.

3. Results and discussion

3.1. Characterization of Con A–$Cu_3(PO_4)_2$ hybrid nanoflowers

The size and appearance of the "self-assembly" nanoflowers were characterized using SEM. As shown in Fig. 1A, the nanostructures were typically flower-like with an average diameter

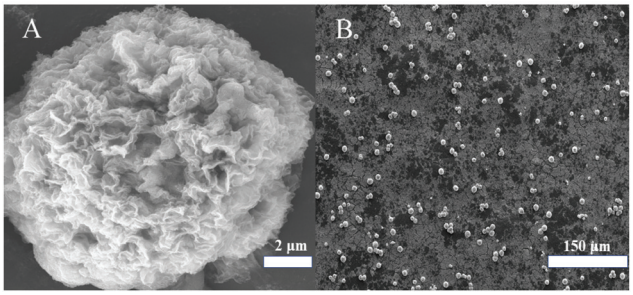

Fig. 1 SEM image of a Con A–$Cu_3(PO_4)_2$ nanoflower.

of about 13 μm. When compared with a terser structure such as a solid sphere or polyhedral region, the nanoflower surface presented numerous folds and a huge surface area for a given volume, resulting in higher surface energy. Furthermore, the nanoflowers comprised uniform spherical structures and had good dispersibility (Fig. 1B); as a result, they exhibited a very good specific surface area. The flower-like material could act as a good carrier material for signal recognition and signal conversion.

3.2. Characterization of the sandwich structure

Both the ends of the aptamer were modified with biotin and fluorescein isothiocyanate (FITC), respectively, while the MBs were modified with SA. The binding of the aptamer to the MBs was realized through the specific recognition of SA and biotin. The aptamer modified with FITC was assayed under a fluorescence microscope. Fig. 2 clearly shows that the MBs (average diameter, 2.8 μm) are fluorescent, indicating that the MBs and the aptamer fitted well together.

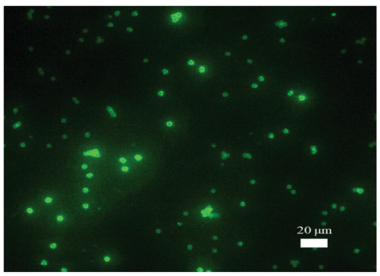

Fig. 2 Fluorescence microscopy image of MBs bound to aptamers.

3.3. Electrochemical characterization of the developed biosensor

The pretreated bare gold electrodes exhibited a couple of well-defined redox peaks of $[Fe(CN)_6]^{3-/4-}$ owing to the efficient electron transfer capability of the sensor surface. However, when G1 was added to the surface of the gold electrode, electron transfer was inhibited and a significant reduction in the CV REDOX peak was observed clearly. The addition of MCH further decreased the CV signal owing to its non-electrical activity. However, in the presence of Cu ions, G1 and G2 formed a G-quadruplex structure and the REDOX peak continued to decrease owing to the hindrance of electron transfer (Fig. 3A). EIS is an important technique for examining modified gold electrodes. Fig. 3 shows the results of EIS performed at 5×10^{-2}–1×10^{6} Hz with an amplitude of 10 mV in $[Fe(CN)_6]^{3-/4-}$ solution. When compared with bare electrodes, the resistance of G1-modified electrodes increased. Following surface blocking with MCH, the resistance of G1-MCH-modified electrodes further increased owing to the insulation property of MCH. As expected, after combination with the G2 fragment, the resistance response curve of the G1-MCH-G2-modified electrodes became larger. These results showed the successful preparation of the biosensor (Fig. 3B). To demonstrate the operability of the prepared sensor, DPV measurements were obtained using the G-quadruplex structure in the absence or presence of the target *S. typhimurium*. Hemin was used for signal amplification, and the hemin-containing G-quadruplex structure was used as the signal label, which produced a significant strong peak current. In contrast, the G-quadruplex structure without hemin generated a weak and negligible electrical signal. This was owing to the lack of bacterial association, the absence of Cu ions, and the inability to form a G-quadruplex structure. Thus, the presence or absence of

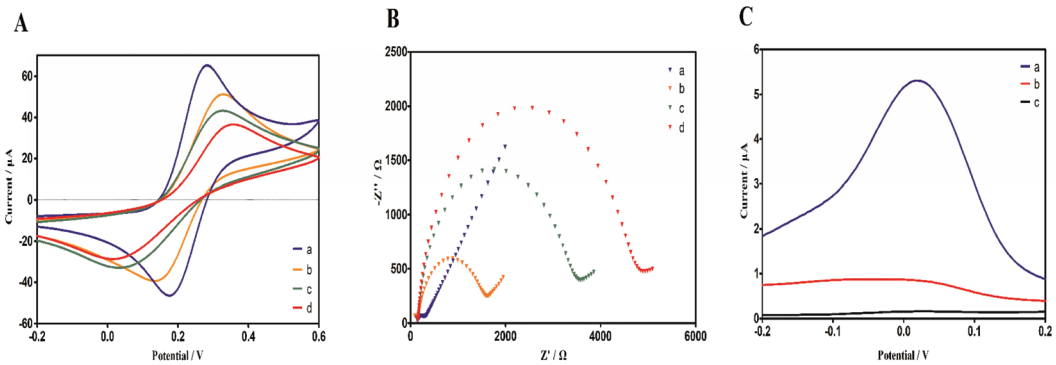

Fig. 3 CV, EIS and DPV of modified gold electrodes. (A) a: bare electrode, b: G1-modified electrode, c: G1-MCH-modified electrode, d: G1-MCH-G2-modified electrode; (B) a: bare electrode, b: G1-modified electrode, c: G1-MCH-modified electrode, d: G1-MCH-G2-modified electrode; (C) typical DPV response: a, Au/G1/MCH/G2 with hemin; b, Au/G1/MCH/G2 without hemin; and c, blank negative control.

hemin had only a minor impact on the electrical signal (Fig. 3C).

3.4. Optimization of the experimental conditions

To improve the sensitivity of the developed biosensor, the concentration of the probe was first optimized because the amount of the probe could directly affect the quantity of the G-quadruplex structure formed. As shown in Fig. 4, the current signal increased with the increase in the concentration of G2 from 0.5 to 1.5 μM. However, when the G2 concentration reached 1.5 μM, the current signal slightly decreased, and a further increase in G2 concentration caused a gradual decrease in the signal intensity, which may be owing to the detrimental effect of a high probe concentration on the formation of the G-quadruplex structure. Hence, 1.5 μM was chosen as the optimal concentration of G2 (Fig. 4A). To improve the performance of the electrochemical biosensor, the hemin concentration was optimized because the amount of hemin could directly affect the intensity of the electrical signal. Accordingly, different concentrations of hemin were added to the reaction system after the formation of the G-quadruplex structure. The electrical signal increased with the increasing concentration of hemin from 5 to 15 μM, but slightly decreased at a hemin concentration higher than 15 μM. Therefore, 15 μM was considered to be the optimal hemin concentration. To achieve the maximum performance of the developed biosensor, the reaction time was optimized to enhance the electrical signal. As shown in Fig. 4B, an increase in incubation time enhanced the electrical signals. When the incubation time reached 60 min, the electrical signal slowly increased, and hence, 60 min was considered as the optimal incubation time (Fig. 4C). As mentioned earlier, the G1 and G2 fragments were modified by the azide group and alkyne group, respectively, and the long strands of DNA could affect the reaction rate between these two groups, resulting in a longer reaction time. Subsequently, the effects of pH were ascertained using phosphate-buffer solution. As shown in Fig. 4D, when pH was 5.5, almost no electrical signal was detected. With the gradual increase in pH, the electrical signal increased, with a pH of 7.5 producing the strongest signal; however, a further increase in pH gradually weakened the electrical signal.

3.5. Sensitivity

The sensitivity and linear range of the developed biosensor for *S. typhimurium* detection were studied under the abovementioned optimal conditions. Fig. 5A presents the susceptive response relationships between *S. typhimurium* concentrations and DPV signals, indicating that the electrical signals strengthened with the increasing bacterial concentration (10^1, 10^2, 10^3, 10^4, 10^5, 10^6, and 10^7 CFU mL^{-1}). The linear equation (Fig. 5B) can be given as follows: $Y = 0.8145 \times X - 0.0219$ ($R^2 = 0.9817$), where Y is the DPV value, X is the concentration (logarithm) of *S. typhimurium*, and R^2 is the correlation coefficient. The electrical signal was particularly low in the absence of bacterial cells. When compared with some previously reported methods (Table 2), these results demonstrated that the developed electrochemical sensor had good sensitivity for the detection of *S. typhimurium.*

3.6. Specificity

The specificity of the electrochemical sensor was determined using various foodborne pathogenic bacteria, including *E. coli* O157:H7, *S. aureus*, and *L. monocytogenes.* As shown in Fig. 6, *S. typhimurium* induced a strong DPV response, whereas *E. coli*

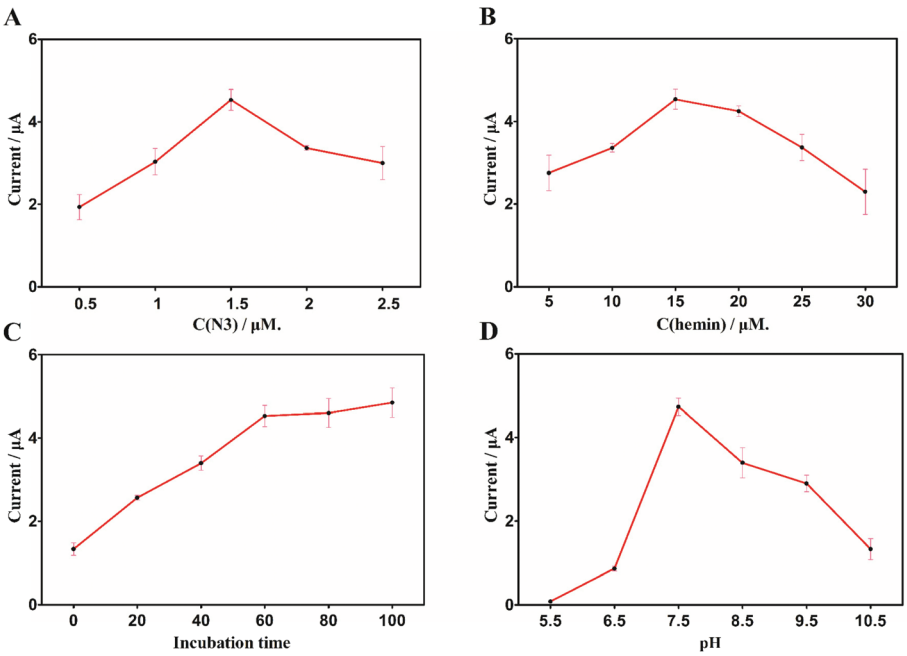

Fig. 4 Optimization of the experimental conditions. (A) G2 concentration; (B) hemin concentration; (C) incubation time; (D) pH.

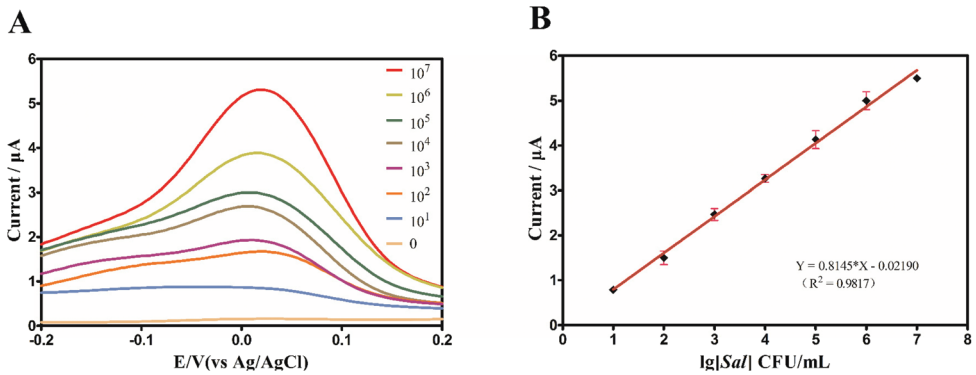

Fig. 5 (A) Typical DPV response of the developed electrochemical biosensor to *S. typhimurium* at different concentrations. (B) Calibration curve of the peak current intensity of DPV *vs.* the logarithm of *S. typhimurium*. Each *S. typhimurium* concentration was assayed in triplicate to generate average values.

Table 2 Comparisons among different methods for *S. typhimurium* determination

Type of biosensor	Detection range (CFU mL^{-1})	Detection limit (CFU mL^{-1})	Ref.
Colorimetric detection	11–1.10×10^5	11	33
Lateral flow immunoassay	10^2–10^8	10^2	34
Impedimetric detection	10^2–10^8	3	35
Fluorescence detection	10^2–10^6	25	36
Electrochemical detection	10^1–10^7	10	This work

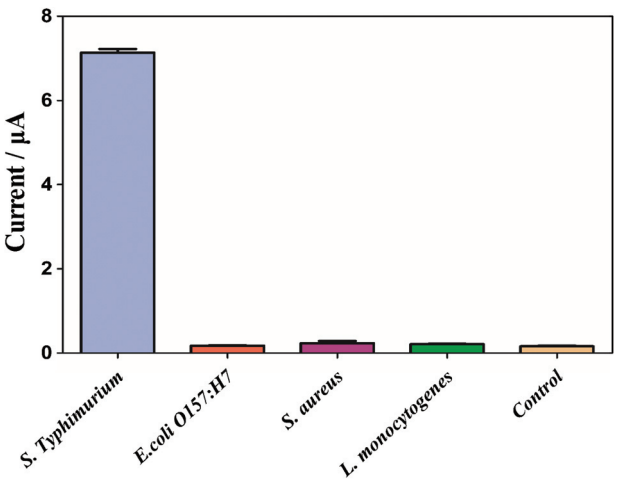

Fig. 6 Specificity of the developed electrochemical biosensor (bacterial cell concentration: 10^7 CFU mL^{-1}). The error bar is the standard deviation of at least three replicates.

O157:H7, *S. aureus*, and *L. monocytogenes* had no significant DPV signals, which were almost the same as those noted in the blank control. These results revealed that the developed electrochemical biosensor presented high specificity to *S. typhimurium.*

3.7. Analysis of milk samples

Milk, which is a major source of proteins, is susceptible to *S. typhimurium* infection. In the present study, various concentrations of *S. typhimurium* were added to aseptic milk to examine the reliability of our developed electrochemical biosensor. As shown in Table 3, the recovery rates ranged from 101% to 107%, indicating that the developed electrochemical sensor is a useful tool for the detection of *S. typhimurium* and the exploration of etiology.

Table 3 Detection of *S. typhimurium* in spiked milk samples

Original value (CFU mL^{-1})	Added (CFU mL^{-1})	Detected (CFU mL^{-1})	Recovery ± RSD (%)
0	1×10^3	1.04×10^3	104 ± 9.7
0	1×10^4	1.07×10^4	107 ± 6.6
0	1×10^5	1.01×10^5	101 ± 12.11

4. Conclusion

A novel label-free electrochemical biosensor was developed in this study for selective and highly sensitive detection of *S. typhimurium* based on $Cu_3(PO_4)_2$-mediated click chemistry and DNAzymes. Owing to the azide reaction, the presence of the target *S. typhimurium* led to the formation of numerous G-quadruplex/hemin DNAzymes on the electrode, thus creating extremely formidable catalytic activity toward H_2O_2 and generating a remarkably strong electrochemical response. Unlike the antibody–enzyme or antibody–CuO conjugate, organic–inorganic hybrid nanoflowers used as the signal producer of the immunoassay were cheap and simple to prepare,

and did not require a complex synthesis procedure. Besides, organic–inorganic hybrid nanoflowers were not susceptible to changes in the external environment (such as pH value and inhibitory effects of bioenzymes), and the Cu^{2+} in the nanoflowers participated in the click chemistry reactions. Hence, the developed electrochemical biosensor could provide a practical and precise platform for highly sensitive and selective detection of pathogenic bacteria in related food safety analysis and clinical diagnoses.

Conflicts of interest

The authors declare that there is no conflict of interest.

References

1 H. C. Kolb, M. G. Finn and K. B. Sharpless, *Angew. Chem., Int. Ed.*, 2001, **32**, 2004–2021.
2 R. S. Gomes, G. A. M. Jardim, R. L. de Carvalho, M. H. Araujo and E. N. da Silva Júnior, *Tetrahedron*, 2019, **75**, 3697–3712.
3 V. V. Rostovtsev, L. G. Green, V. V. Fokin and K. B. Sharpless, *J. Cheminf.*, 2002, **14**, 2596–2599.
4 M. Tarnowska and T. Krawczyk, *Biosens. Bioelectron.*, 2020, **169**, 112614.
5 S. Zhang, W. Yi, Y. Guo, R. Jiang, X.-L. Chen, B. Yang and J. Wang, *ACS Appl. Nano Mater.*, 2021, **4**, 4623–4631.
6 C. W. TornøE, C. Christensen and M. Meldal, *J. Org. Chem.*, 2002, **67**, 3057–3064.
7 Y. Rondelez, M.-N. Rager, A. Duprat and O. Reinaud, *J. Am. Chem. Soc.*, 2002, **124**, 1334–1340.
8 P. Thirumurugan, D. Matosiuk and K. Jozwiak, *Chem. Rev.*, 2013, **113**, 4905–4979.
9 M. Kiani, M. Bagherzadeh, S. Meghdadi, F. Fadaei-Tirani, M. Babaie and K. Schenk-Joß, *Inorg. Chim. Acta*, 2020, **506**, 3442–3445.
10 M. Ito, T. Ootsuka, R. Watari, A. Shiibashi, A. Himizu and T. Ikariya, *J. Am. Chem. Soc.*, 2011, **133**, 4240–4242.
11 W. Qu, Y. Liu, D. Liu, Z. Wang and P. Zhuo Wang, *Angew. Chem., Int. Ed.*, 2011, **50**, 3442–3445.
12 Q. Xie, X. Weng, L. Lu, Z. Lin, X. Xu and C. Fu, *Biosens. Bioelectron.*, 2016, **77**, 46–50.
13 A. S. Naeemi, F. Elmi, G. Vaezi and M. Ghorbankhah, *Gene Rep.*, 2020, **19**, 100676.
14 Y. Liu, M. Du, J. Zhu, X. Hu, X. Ji and Z. He, *ACS Appl. Nano Mater.*, 2018, **1**, 4964–4971.
15 S. K. Rai, L. K. Narnoliya, R. S. Sangwan and S. K. Yadav, *ACS Sustainable Chem. Eng.*, 2018, **6**, 6296–6304.
16 L. Zheng, X. Xie, Z. Wang, Y. Zhang, L. Wang, X. Cui, H. Huang and H. Zhuang, *Green Chem. Lett. Rev.*, 2018, **11**, 55–61.
17 T. D. Tran and M. I. Kim, *BioChip J.*, 2018, **12**, 268–279.
18 C. Ke, Y. Fan, Y. Chen, L. Xu and Y. Yan, *RSC Adv.*, 2016, **6**, 19413–19416.
19 X. Lang, L. Zhu, Y. Gao and I. Wheeldon, *Langmuir*, 2017, **33**, 9073–9080.
20 C. Ke, Y. Fan, Y. Chen, L. Xu and Y. Yan, *RSC Adv.*, 2016, **6**, 19413–19416.
21 M. Chung, T. L. Nguyen, T. Q. N. Tran, H. H. Yoon, I. T. Kim and M. I. Kim, *Appl. Surf. Sci.*, 2018, **429**, 203–209.
22 B. Somturk, I. Yilmaz, C. Altinkaynak, A. Karatepe, N. Ozdemir and I. Ocsoy, *Enzyme Microb. Technol.*, 2016, **86**, 134–142.
23 S. Wang, Y. Ding, R. Chen, M. Hu, S. Li, Q. Zhai and Y. Jiang, *Chem. Eng. Res. Des.*, 2018, **134**, 52–61.
24 Q. Tang, L. Zhang, X. Tan, L. Jiao, Q. Wei and H. Li, *Biosens. Bioelectron.*, 2019, **133**, 94–99.
25 T. Wu, Y. Yang, Y. Cao, Y. Song, L. P. Xu, X. Zhang and S. Wang, *ACS Appl. Mater. Interfaces*, 2018, **10**, 42050–42057.
26 J. Gao, H. Liu, L. Pang, K. Guo and J. Li, *ACS Appl. Mater. Interfaces*, 2018, **10**, 30441–30450.
27 Z. Zhang, T. Li, Y. Sheng, L. Liu and H.-C. Wu, *Small*, 2018, **15**, 1804078.
28 D. Li, J. Xie, W. Zhou, B. Jiang, R. Yuan and Y. Xiang, *Anal. Bioanal. Chem.*, 2017, **409**, 6421–6427.
29 Y. Fu, X. Zhou, X. Duan, C. Liu, J. Huang, T. Zhang, S. Ding and X. Min, *Sens. Actuators, B*, 2020, **321**, 128502.
30 Y. Chen, Y. Xianyu, J. Wu, B. Yin and X. Jiang, *Theranostics*, 2016, **6**, 969–985.
31 N. F. D. Silva, J. Magalhaes, C. Freire and C. Delerue-Matos, *Biosens. Bioelectron.*, 2018, **99**, 667–682.
32 J. M. Eijkelkamp, H. J. M. Aarts and H. J. van der Fels-Klerx, *Food Anal. Methods*, 2008, **2**, 1–13.
33 S. Wu, N. Duan, Y. Qiu, J. Li and Z. Wang, *Int. J. Food Microbiol.*, 2017, **261**, 42–48.
34 Z. Wang, X. Yao, R. Wang, Y. Ji, T. Yue, J. Sun, T. Li, J. Wang and D. Zhang, *Biosens. Bioelectron.*, 2019, **132**, 360–367.
35 E. Sheikhzadeh, M. Chamsaz, A. P. F. Turner, E. W. H. Jager and V. Beni, *Biosens. Bioelectron.*, 2016, **80**, 194–200.
36 X. Wang, S. Niazi, H. Yukun, W. Sun, S. Wu, N. Duan, X. Hun and Z. Wang, *Microchim. Acta*, 2017, **184**, 4021–4027.